

Full paper

# Biomechanical Approach to Open-Loop Bipedal Running with a Musculoskeletal Athlete Robot

Ryuma Niiyama <sup>a,\*</sup>, Satoshi Nishikawa <sup>b</sup> and Yasuo Kuniyoshi <sup>c</sup>

<sup>a</sup> Computer Science and Artificial Intelligence Laboratory, Massachusetts Institute of Technology, Cambridge, MA 02129, USA

<sup>b</sup> Graduate School of Interdisciplinary Information Studies, University of Tokyo, Bunkyo-ku, Tokyo 113-0033, Japan

<sup>c</sup> Graduate School of Information Science and Technology, University of Tokyo, Bunkyo-ku, Tokyo 113-0033, Japan

Received 12 August 2011; accepted 16 September 2011

## Abstract

In this study, a musculoskeletal robot is used as a tool to investigate how animals control their complex body. Sprinting is a challenging task that requires maximizing the potential resources of a musculoskeletal structure. Our approach to robotic sprinting is the Athlete Robot — a musculoskeletal robot with elastic blade feet controlled by feedforward motor command. We use a catapult launcher to provide a stable start to a sprint, and then examine the relation between the initial velocity imparted by the launcher and the change in orientation of the robot. We also investigate the influence of the change in elasticity of the blade foot. The results show that acceleration causes anterior inclination after the first step. The elasticity of the foot dominates the duration of the support phase. The musculoskeletal system of the Athlete Robot is modified to suit catapulted running. Based on the results from real robot experiments, we can provide a consistent propelling force using the catapult launcher. We demonstrate the Athlete Robot running for five steps after a catapult launch, using only feedforward command.

© Koninklijke Brill NV, Leiden and The Robotics Society of Japan, 2012

## Keywords

Legged locomotion, musculoskeletal system, pneumatic, biomechanics, running

## 1. Introduction

The dynamic movement and the agile legged locomotion of animals are very important subjects from the perspective of the efficiency and control of complex nonlinear systems. In particular, running is a challenging task that entails maximization of the

\* To whom correspondence should be addressed. E-mail: ryuma@csail.mit.edu

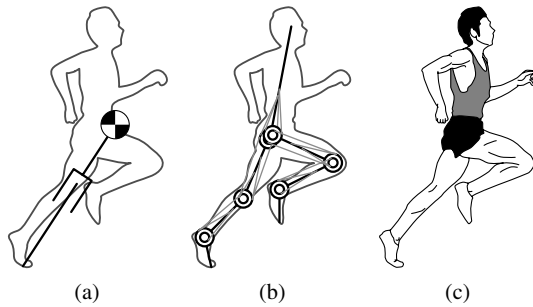


**Figure 1.** Utilization of the musculoskeletal system in human running. (a) Inverted pendulum. (b) Musculoskeletal. (c) Human body.

capacity of a robot. Although previous studies on a hopping robot presented the basics for legged locomotion using a simple mechanism [1], animal locomotion based upon a musculoskeletal system (Fig. 1) is not well understood.

The control of the ground reaction force plays a major role in legged locomotion in terms of providing the propelling force and maintaining a posture. There are several humanoid robots capable of bipedal running [2, 3], but only a few robots employ a hardware design for force control [4, 5]. The hydraulic-powered biped PETMAN and the Atlas developed by Boston Dynamics are operated using the force control utilized in the quadruped robot BigDog [6]. The function of elasticity of tissue in dynamic movement is recognized in the field of biomechanics [7], and biological insights suggest that utilizing the passive dynamics of the body, including elasticity, improve the performance of a legged robot. However, only a few applications of a musculoskeletal system in legged robots have been studied to date. The Kotaro and Kojiro robot is a full-size humanoid robot driven by a number of wire tension actuators [8]. The robot mainly demonstrates the advantages of flexibility derived from a redundant layout of actuators and a flexible spine structure. Lucy is another bipedal musculoskeletal robot driven by an antagonistic mechanism using a pair of pneumatic muscles [9], but has only monoarticular muscles. The robot uses zero-moment point (ZMP)-based motion planning for walking with joint angle control. Another study concerns an anthropomorphic musculoskeletal robot [10], which performs quasi-passive walking, hopping and dash of a few steps. This robot has a limitation, which is controlling air flow using the on/off function of solenoid valves.

Our objective is to study sprinting by a musculoskeletal Athlete Robot based on the anatomical structure of a human being. The robot is driven by pressure-controlled pneumatic muscles, and also has monoarticular and biarticular muscles. A human athlete can sprint from a block start. The sprint start is one of the skills that provide initial velocity and potential energy for the runner. We propose the use of a catapult launcher to replace the skills of the sprint start. In this study, we focus more on experiments using a real robot than on dynamic simulations. This is because issues such as uncertain contact, limited response of the actuators and restricted resources for computation are considerable constraints to understand the principles of animal locomotion.

## 2. Athlete Robot

### 2.1. Musculoskeletal Athlete Robot

The Athlete Robot is a bipedal robot designed for sprinting using a biomechanical approach [11]. The robot weighs about 10 kg. The body height, length of thigh and shank are 1.2, 0.3 and 0.36 m, respectively (Fig. 2). The human body is comprised of unique mechanisms such as elastic tendons, biarticular muscles and antagonistic drive. Like the human body, the Athlete Robot has an artificial musculoskeletal system that mimics the anatomical structure of the human body (Fig. 3 and Table 1). The elasticity of the tendons around the ankle joint is simply implemented as an elastic blade. The pneumatic muscle actuators used for the system allow agile

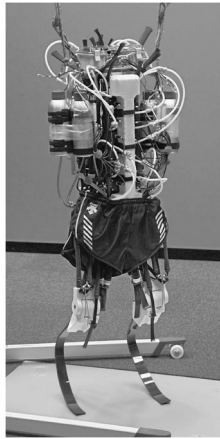


**Figure 2.** Musculoskeletal Athlete Robot.

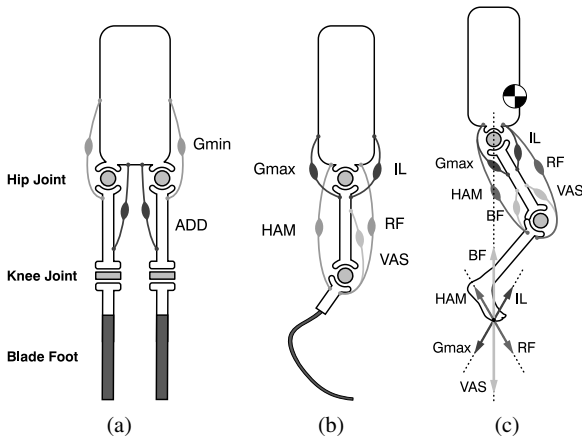


**Figure 3.** Layout of the muscles. Gmin, gluteus minimus muscle; ADD, adductor muscles; Gmax, gluteus maximus muscle; IL, iliopsoas muscle; HAM, hamstrings; RF, rectus femoris muscle; VAS, vastus muscles. (a) Front view. (b) Side view. (c) Force output.

**Table 1.**

Parameters for the musculoskeletal system: size of member muscles, number of muscles in each muscle group and moment arms on each joint

Muscle group	$d_0$ (m)	$l_{\max}$ (m)	No. of muscles	$D_{\text{hip}}$ (m)	$D_{\text{knee}}$ (m)
ADD	0.008	0.180	2	0.050	—
Gmin	0.008	0.256	2	0.050	—
Gmax	0.005	0.256	6	0.028–0.040	—
IL	0.005	0.256	2	0.028–0.040	—
HAM	0.005	0.160	2	0.020–0.040	0.028
RF	0.005	0.200	1	0.025	0.028
VAS	0.005	0.160	2	—	0.028

$d_0$ , initial diameter of the muscle;  $l_{\max}$ , maximal length of the muscle;  $D_{\text{hip}}$ , moment arm on hip joint;  $D_{\text{knee}}$ , moment arm on knee joint.

and compliant movement of the robot. Although the pneumatic actuator is not suitable for precise position/angle control, force/torque control can be easily achieved by using pressure control. We employ custom-made proportional control valves to control the inner pressure of the muscles. The robot is equipped with a miniature computer, valves and an accumulator. Electric power and compressed air are provided by external equipment. A contact sensor for each foot, a pressure sensor for each muscle and an inertia measurement unit (IMU) are available for measurement.

## 2.2. Catapult Launcher

To provide the initial velocity for running, we use a catapult launcher (Fig. 4). An air cylinder with a diameter of 32 mm and a stroke of 200 mm generates the pneumatic thrust force. The initial velocity can be determined by regulating the air supply range of 0.0–0.9 MPa. Roller sliders attached to the robot and double linear guide rails on the launcher allow smooth acceleration. The air cylinder is connected to a solenoid valve operated by a push-button switch. The robot can detect the time of launch by using a limit switch. To ensure a stable launch, the catapult launcher has a weighted base, which is fixed to the floor with an adhesive medium.

## 3. Design of the Athlete Robot

### 3.1. Simulation Setup

In order to investigate appropriate parameters of the robot adapted to use in a catapult launcher, we use a dynamic simulation. In particular, we optimize the number of muscles and the spring property of the elastic blade foot by means of a dynamic simulation using OpenHRP3 [12]. The physical parameters of the body parts are calculated from the 3DCAD models. Data on the shape of the blade foot used for detecting ground contact in the simulator are also imported from 3DCAD. Figure 5 shows a geometric model and a configuration of the degrees of freedom of the robot

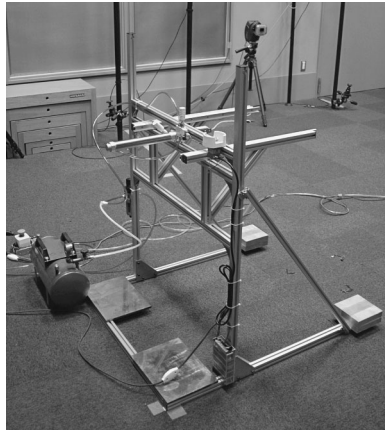
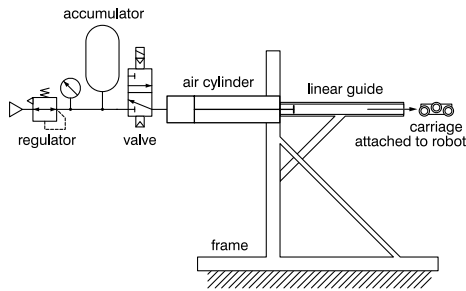


**Figure 4.** Catapult launcher actuated by a pneumatic piston. The pneumatic circuit provides a constant air supply.

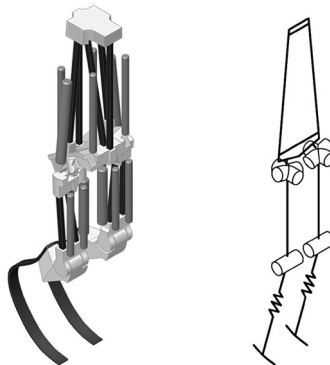


**Figure 5.** Geometric model used for collision detection and the configuration of the joints of the Athlete Robot.

for the simulation. We modeled the elastic bending of the blade foot as a translational spring. A theoretical model and characterization of pneumatic muscles is presented in Ref. [13]. We also take account of the delay in pressure response and an energy loss based upon the pilot study.

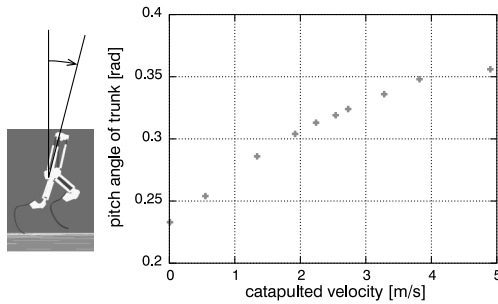


**Figure 6.** Simulation study of posture with different initial velocities.

### 3.2. Muscular System

The robot has monoarticular muscle groups and biarticular muscle groups corresponding to the major muscles of the lower extremities of a human body. Each muscle group consists of several muscles. We determined the parameters for the moment arm of each muscle group and the number of muscles in a group based upon the data in biomechanics [14, 15]. The number of muscles in each muscle group is critical for the Athlete Robot because it uses almost 100% of the maximum force output. To achieve faster running, we have to provide additional muscles to the robot. It is expected that an inadequate number of muscles would cause a loss of balance and in ability to support its own weight. On the other hand, there is a trade-off between the number of muscles and the increase in weight of the additional valves.

We investigate the relation between the initial velocity imparted by the catapult launcher and the rotation of the trunk after the first step (Fig. 6). The result shows that anterior inclination of the trunk increases with an increase in the initial velocity. Thus, an adjustment of the ground reaction force is required to avoid the robot falling as a result of forward rotation. The relation between the muscle tension force and the output force on the end-effector can be described by using a Jacobian matrix [16, 17]. Figure 3c shows the force components acting upon the foot corresponding to each muscle. The Gmax gluteus is responsible for preventing the robot from leaning forward around the center of mass. Therefore, we increased the number of members of the Gmax muscle group from four to six in each leg. Figure 7 shows the strength of each muscle and a comparison with human data.

### 3.3. Blade Foot

The tendons in the human lower leg play crucial roles in energy storage and impact absorption. In the robotic arm literature, elastic elements have been employed both for their force control and their compliance [18]. Passive, compliant legs have also been used for agile multi-legged robots, inspired by insect locomotion [19, 20]. Biomechanical studies indicate that the human lower leg behaves in the same manner as a spring during dynamic movement [21, 22]. In addition, a human athlete using running-specific prostheses can perform sprinting that is close in performance

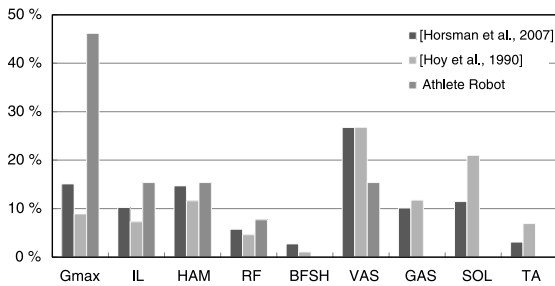


**Figure 7.** Strength of each muscle and comparison with human data (Horsman *et al.* [15] and Hoy *et al.* [14]). The values are expressed as percentages of the total maximal output force.

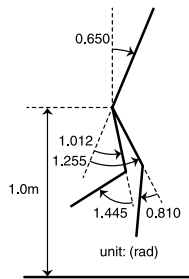


**Figure 8.** Initial posture for the kick and bounce simulation study.

to that of able-bodied people [23]. Therefore, we designed the robot foot as an elastic blade.

We tested the effect of changes in the spring property through simulation experiments. We performed a mono-leg bounce from a drop height of 1.0 m in a static posture (Fig. 8). The posture of the robot is sustained by antagonistic activity of the muscles. The muscle activation for the stance leg is set as:

$$\begin{aligned}
 P_{\text{thrust}} &= K [P_{G\text{min}} P_{\text{ADD}} P_{G\text{max}} P_{\text{IL}} P_{\text{HAM}} P_{\text{RF}} P_{\text{VAS}}]^T \\
 &= K [0.15 \ 0.10 \ 0.90 \ 0.00 \ 0.90 \ 0.90 \ 0.90]^T \text{ (MPa)}.
 \end{aligned}$$

In this experiment, we change the kicking strength by using different weights of  $K = 1.0, 0.8, 0.6, 0.4$  and  $0.2$  with various spring constants. The result shows that the spring constant of the blade foot is dominant for the time period from ground contact to takeoff (Fig. 9). In other words, thrust strength does not have a significant effect on contact time. Meanwhile, the amplitude of velocity on takeoff depends upon the applied thrust strength (Fig. 10). The control range of the takeoff velocities decreases with the increase in spring constant. A small spring constant causes the robot to fall before bouncing. Although a short contact time is desirable to maximize the pitch and stride of running, the robot has a limited time constant in the pneumatic system. We chose a spring constant of 6125 N/m for the blade foot to maximize the control range of the takeoff velocity under the limited response of the pneumatic system. We modified prosthetic legs intended for a human athlete

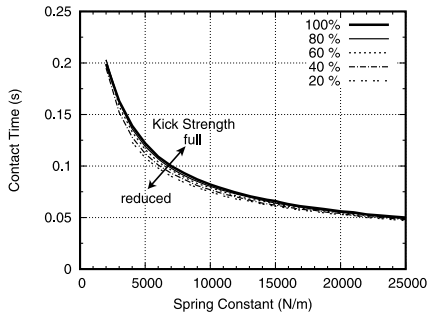


**Figure 9.** Simulation kick and bounce study. The relation between the duration of the support phase and the spring constant of the blade foot is shown.

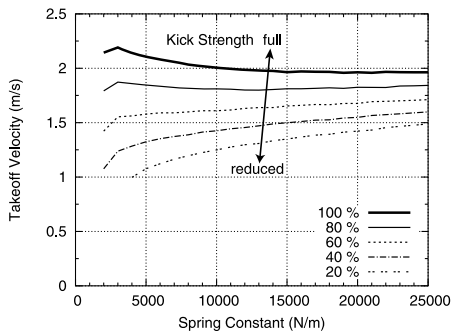


**Figure 10.** Simulation kick and bounce study. The relation between the takeoff velocity and spring constant of the blade foot is shown.

(Ossur, Flex Foot Cheetah) for the robotic feet. The reported stiffness of the human Achilles tendon is about  $150\text{--}200 \times 10^3 \text{ Nm}^{-1}$  under *in vivo* condition [22]. We can scale the stiffness for the robot by using body weight. The converted stiffness for the robot becomes  $5250\text{--}7250 \text{ Nm}^{-1}$ , if we assume a 70-kg human subject and a 1:4 leverage ratio for the ankle joint. The actual stiffness of the blade foot of the robot is within the range.

## 4. Running Experiments

### 4.1. Motor Command Generation

We used a dynamic simulator to model bipedal running from a catapult-assisted launch prior to conducting actual robot experiments. The launcher is modeled as a horizontal thrust joint connected to the trunk of the robot. The motor command for running is derived from exploration and optimization through trials. The combination of constrained random sampling and hill-climbing optimization is used to obtain a muscle activation pattern for running. We use binarized human electromyography (EMG) data as the constraint for random sampling.

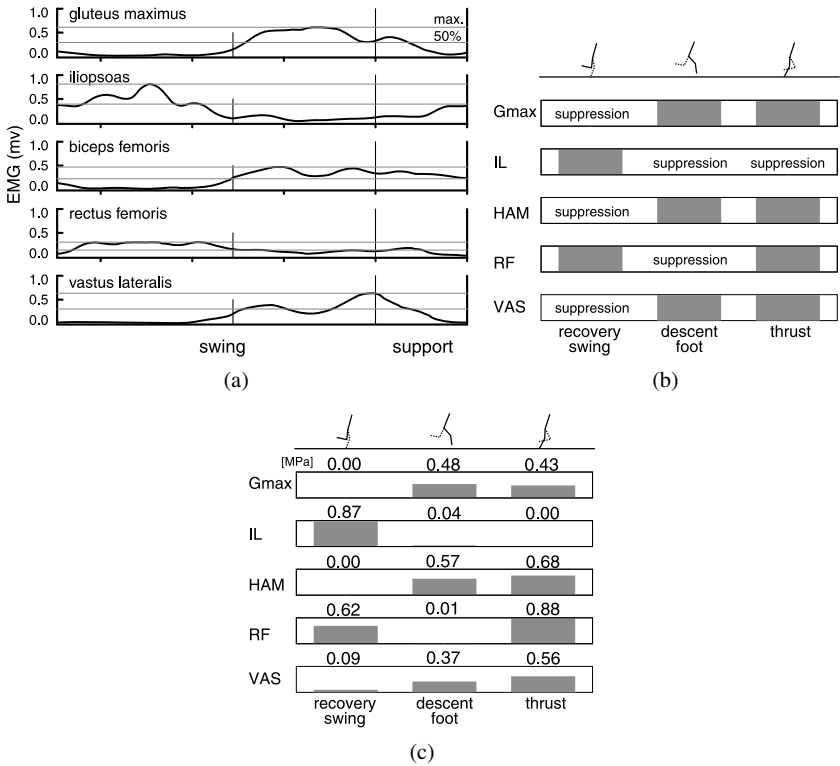


**Figure 11.** Muscle activation pattern through trials and binarized EMG patterns. (a) EMG data during running. (b) Binarized EMG for random sampling. (c) Optimized muscle activation pattern.

A running gait cycle consists of two major phases: a thrust (support) phase and a swing phase. We divide the swing phase into two phases: a recovery swing phase and a foot-descent phase based on the presence of a zero crossing of hip joint torque in kinetic data on human running. The continuous EMG profile of each muscle is binarized with a threshold on each phase as shown in Fig. 11b. The threshold is set to the half-peak voltage of the EMG signal for each muscle. In a subsequent random sampling for the generation of initial values for hill-climbing search, a signal with a zero level in the binarized EMG means a suppression to zero. From the results of the kick and bounce experiments, the duration of the thrust phase is determined by the stiffness of the blade foot. The total length of the aerial phase is determined by the takeoff velocity. Therefore, we have to search only for the ratio between recovery swing and foot descent. Eventually, the parameters for exploration are: muscle activation level for five muscle groups at each phase, the splitting ratio of aerial phase and the start time for motor command after launch.

Figure 11c shows an acquired best muscle activation pattern obtained through a 300-point random sampling and 150-step hill-climbing optimization based upon human EMG data during running [24–26]. The length of the aerial phase is estimated by using the adjacent takeoff velocity. The initial velocity of the robot is

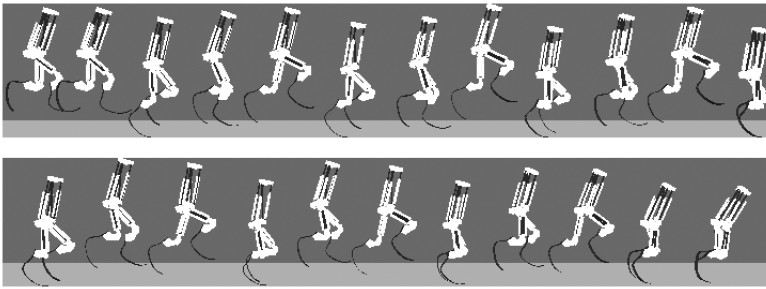


**Figure 12.** Images from a running simulation taken at 0.3-s intervals using the best parameters.

set to 2.0 m/s. The robot achieved 13 running steps with 12.5 m of forward travel (Fig. 12). The mean velocity of the robot was about 2.1 m/s. The learned percentage of the descent foot phase was 32% of the total swing phase. The simulations predict that the robot can successfully run more than 10 steps at feedforward control using simplified muscle activation patterns.

#### 4.2. *Single Muscle Activation*

As a pilot study, we measured the ground reaction force corresponding to the activation of a single muscle by using a force plate. The robot was suspended from a ceiling beam, with the legs touching the force plate. We recorded the motion using a Vicon motion capture system and Kistler force plates. The initial ground reaction force is reset to zero. Then we applied pressure to a particular muscle. As shown in Fig. 13, the measured ground reaction force is consistent with the theoretical prediction. The VAS muscle generates force directed to the hip joint and a Gmax muscle generates forces directed to the knee joint. The results show that we can directly control the direction of the ground reaction force by muscle activation.

#### 4.3. *Real Robot Experiment*

We investigate the operating conditions of the catapult launcher as the first step to obtain the desired starting velocity for the robot. Figure 14 shows the resultant forward velocities with various supply pressures. The results show that the initial velocity of the robot corresponds to the supply pressure. The observed saturation of a high supply pressure is due to the limitation of the flow rate. We set the target initial velocity to 2.0 m/s based on the findings of the simulation study. We also evaluate the repeatability of the launcher. The results of the 10 trials show the deviation in velocity is within  $\pm 5\%$  of the desired velocity, as shown in Fig. 15. A stable launch is essential for good subsequent running movement.

A series of running experiments were conducted with the real Athlete Robot. The experiments required 20 trials for the manual modification of the muscle activation pattern given by the simulation. In particular, we changed the scale of the motor command to deal with modeling errors of weight and ground contact. Although the simulation uses information on the length of the aerial phase estimated from takeoff

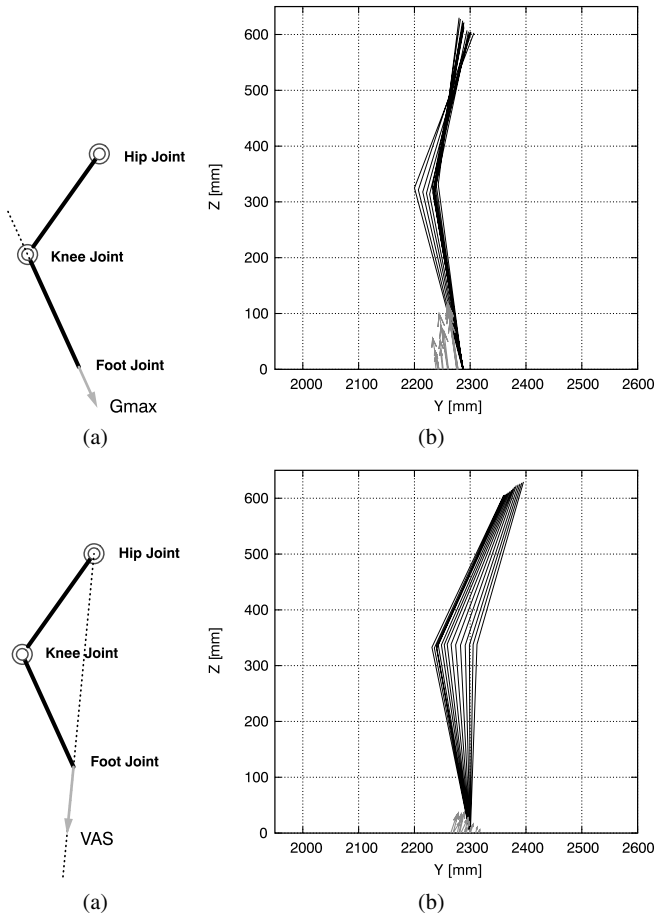


**Figure 13.** Measured ground reaction force for the VAS muscle. (a) Theoretical force output. (b) Measured reaction force.

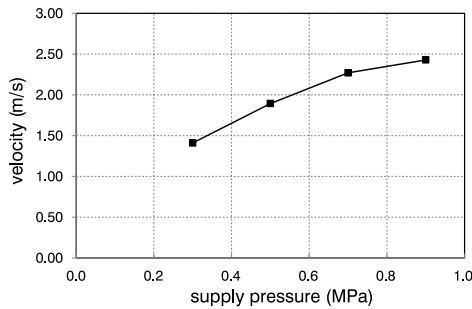


**Figure 14.** Forward velocity of a launched real robot attained before landing corresponding to different supply pressures.

velocity, we manually determined the length through trials due to the poor signal-to-noise ratio of the IMU data. The movements of the body segments are measured

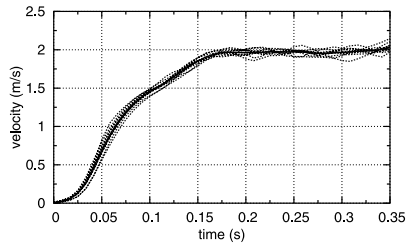


**Figure 15.** Velocity profiles for 10 launches of a real robot with a supply pressure of 0.5 MPa. The bold line is the median of the 10 trials. The position of the marker is recorded with a sampling rate of 120 Hz and processed by a filter with a cut-off frequency of 15 Hz.

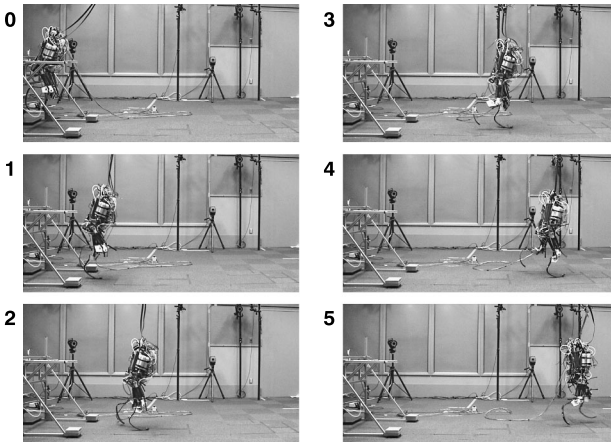


**Figure 16.** Photographs of the robot running five steps.

using a Vicon motion capture system. The ground reaction forces are measured with three force plates. We used rubber sheeting on the soles of the robot's feet and conducted the experiments on a carpeted floor. We also fitted a rubber suspender to the robot, which is slack during running to prevent damage to the robot in case it fell. The Athlete Robot could achieve five running steps and travel a distance of about 4 m at a mean velocity of 2.42 m/s (8.7 km/h). The Froude number for legged locomotion [27] is estimated as  $Fr = v^2/gl = 0.90$ , where  $v$  is the velocity,  $g = 9.80 \text{ m/s}^2$  is the gravity acceleration and  $l = 0.663 \text{ m}$  is the leg length. Figure 16 shows photographs of the robot sprinting from the catapult launcher.

#### 4.4. Results and Discussion

The forward velocity and the ground reaction force during bipedal running (Fig. 16) are shown in Figs 17 and 18. The velocity profile represents a smooth transition to steady running from the launch. The robot starts running at a constant velocity on the second and third step. The forward speed decreases on the fourth step and the robot falls after the fifth step. The elastic blade foot generated bell-shaped vertical ground reaction forces with no impulsive component. The blade foot stored energy

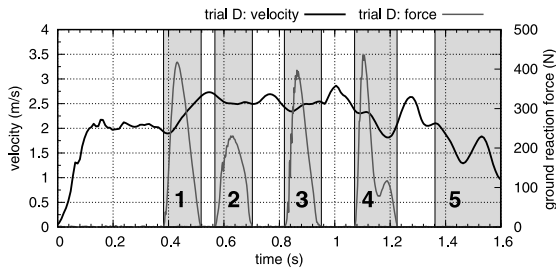


**Figure 17.** Forward velocity of the five running steps. The shaded regions represent support phases with ground contact. The position of the marker is recorded with a sampling rate of 120 Hz and processed by a filter with a cut-off frequency 15 Hz. The force data were sampled at a rate of 600 Hz and processed by a filter with a cut-off frequency of 60 Hz.

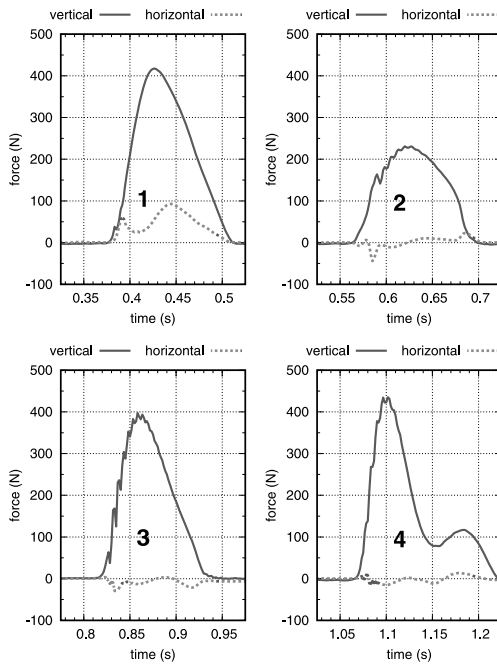


**Figure 18.** Ground reaction force of the steps. The force data were sampled at a rate of 600 Hz and processed by a filter with a cut-off frequency of 60 Hz.

during the first half of the supporting phase and released it during the second half. The positive part of the horizontal force means acceleration. We believe the double peak in the ground reaction force of the fourth step indicates an unsuccessful support attempt. The fifth step occurred outside of the force plates. Rotation around the yaw axis was ignorable due to the small mass on the toe and the small distance of the hip joints.

The applied muscle activation patterns and measured pressures of the muscles are shown in Fig. 19. Muscle activation strength rises predictively prior to ground

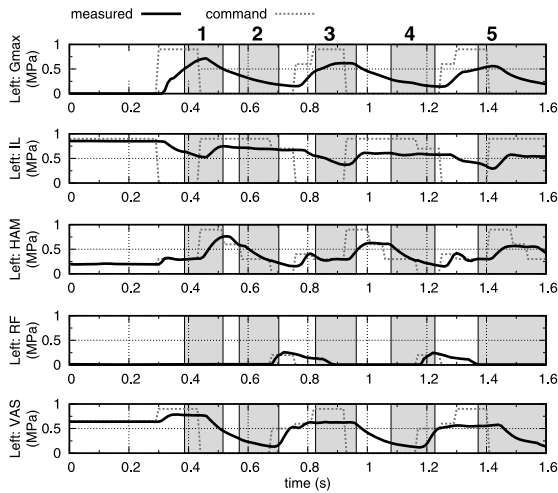


**Figure 19.** Applied muscle activation patterns and measured pressures corresponding to the muscles of the left leg. The shaded regions represents support phases with ground contact.

contact. The optimized motor command takes account of the delays in pressure response of the muscles. We observed that a time lag between motor command and actual ground contact resulted in insufficient support for the robot and in the robot falling in later steps. The skilled movement of sprinting was successfully generated from the simplified muscle activation patterns-based on the human EMG data. The results show that feedforward control can play a significant role in agile movements.

## 5. Conclusions

We proposed a biomechanical approach to bipedal running with a musculoskeletal Athlete Robot using a catapult launcher. The catapult launcher duplicates the skilled sprint start of a human begin and enables detailed analysis of steady running. We investigated the relation between initial velocity and body rotation after the first step. We found that an increase in launch speed causes forward tilting. We also discussed the characteristics of the robot's elastic blade foot during the support phase. The result shows that the spring constant of the blade foot dominates the duration of the support phase. The muscle activation patterns for sprinting were generated by exploration and optimization through dynamic simulation. We demonstrated that the robot can run five steps at a velocity of 2.42 m/s (8.7 km/h) using an open-loop motor command. The ground reaction force during running presented a bell-shaped profile without impulse despite using simplified muscle activation patterns. The results showed the significant contribution made by an elastic lower limb and predictive motor command in agile legged locomotion.

The use of sensory information to supplement feedforward motor commands will be the subject of future work. Extending this method of running to various speeds and steering control will also be explored in future research.

## References

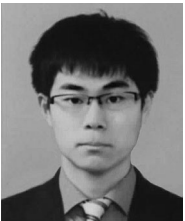
1. M. H. Raibert, *Legged Robots That Balance*. MIT Press, Cambridge, MA (1986).
2. R. Tajima, D. Honda and K. Suga, Fast running experiments involving a humanoid robot, in: *Proc. IEEE Int. Conf. on Robotics and Automation*, Osaka, pp. 1571–1576 (2009).
3. T. Takenaka, T. Matsumoto, T. Yoshiike and S. Shirokura, Real time motion generation and control for biped robot — 2nd report: Running gait pattern generation, in: *Proc. IEEE/RSJ Int. Conf. on Intelligent Robots and Systems*, St Louis, MO, pp. 1092–1099 (2009).
4. S. H. Hyon, Compliant terrain adaptation for biped humanoids without measuring ground surface and contact forces, *IEEE Trans. Robotics* **25**, 171–178 (2009).
5. B. J. Stephens and C. G. Atkeson, Dynamic balance force control for compliant humanoid robots, in: *Proc. IEEE/RSJ Int. Conf. on Intelligent Robots and Systems*, Taipei, pp. 1248–1255 (2010).
6. M. Raibert, K. Blankespoor, G. Nelson, R. Playter and The BigDog Team, BigDog the rough-terrain quadruped robot, in: *Proc. 17th World Congr. of the International Federation of Automatic Control*, Seoul, pp. 10822–10825 (2008).
7. R. M. Alexander and H. C. Bennet-Clark, Storage of elastic strain energy in muscle and other tissues, *Nature* **265**, 114–117 (1977).
8. I. Mizuuchi, Y. Nakanishi, Y. Sodeyama, Y. Namiki, T. Nishino, N. Muramatsu, J. Urata, K. Hongo, T. Yoshikai and M. Inaba, An advanced musculoskeletal humanoid kojiro, in: *Proc. 7th IEEE–RAS Int. Conf. on Humanoid Robots*, Pittsburgh, PA, pp. 294–299 (2007).
9. B. Verrelst, R. V. Ham, B. Vanderborght, F. Daerden, D. Lefeber and J. Vermeulen, The pneumatic biped ‘Lucy’ actuated with pleated pneumatic artificial muscles, *Autonomous Robots* **18**, 201–213 (2005).
10. K. Hosoda, T. Takuma, A. Nakamoto and S. Hayashi, Biped robot design powered by antagonistic pneumatic actuators for multi-modal locomotion, *Robotics Autonomous Syst.* **56**, 46–53 (2008).
11. R. Niiyama and Y. Kuniyoshi, Design of a musculoskeletal athlete robot: a biomechanical approach, in: *Proc. 12th Int. Conf. on Climbing and Walking Robots and the Support Technologies for Mobile Machines*, Istanbul, pp. 173–180 (2009).
12. F. Kanehiro, H. Hirukawa and S. Kajita, Openhrp: open architecture humanoid robotics platform, *Int. J. Robotics Res.* **23**, 155–165 (2004).
13. H. F. Schulte, D. F. Adamski and J. R. Pearson, Characteristics of the braided fluid actuator, Technical Report 5, Department of Physical Medicine and Rehabilitation Orthotics Research Project, University of Michigan Medical School, Ann Arbor, MI (1961).
14. M. G. Hoy, F. E. Zajac and M. E. Gordon, A musculoskeletal model of the human lower extremity: the effect of muscle, tendon, and moment arm on the moment-angle relationship of musculotendon actuators at the hip, knee, and ankle, *J. Biomech.* **23**, 157–169 (1990).
15. M. D. K. Horsman, H. F. J. M. Koopman, F. C. T. van der Helm, L. P. Pros and H. E. J. Veeger, Morphological muscle and joint parameters for musculoskeletal modelling of the lower extremity, *Clin. Biomech.* **22**, 239–247 (2007).
16. K. Ito, T. Tsuji and M. Nagamachi, Motor impedance and inverse kinematics in musculoskeletal systems, in: *Proc. 10th Annu. Int. Conf. of the IEEE Engineering in Medicine & Biology Society*, New Orleans, LA, pp. 635–636 (1988).
17. T. Oshima, T. Fujikawa, O. Kameyama and M. Kumamoto, Robotic analyses of output force distribution developed by human limbs, in: *Proc. 9th IEEE Int. Workshop on Robot and Human Interactive Communication*, Osaka, pp. 400–404 (2000).
18. A. Edsinger-Gonzales and J. Weber, Domo: a force sensing humanoid robot for manipulation research, in: *Proc. 4th IEEE/RAS Int. Humanoid Robots Conf.*, Santa Monica, CA, pp. 273–291 (2004).

19. N. Neville, M. Buehler and I. Sharf, A bipedal running robot with one actuator per leg, in: *Proc. IEEE Int. Conf. Robotics and Automation*, Orlando, FL, pp. 848–853 (2006).
20. S. Kim, J. E. Clark and M. R. Cutkosky, iSprawl: design and tuning for high-speed autonomous open-loop running, *Int. J. Robotics Res.* **25**, 903–912 (2006).
21. T. Fukunaga, K. Kubo, Y. Kawakami, S. Fukashiro, H. Kanehisa and C. N. Maganaris, *In vivo* behaviour of human muscle tendon during walking, *Proc. Roy. Soc. B* **268**, 229–233 (2001).
22. G. A. Lichtwark and A. M. Wilson, *In vivo* mechanical properties of the human achilles tendon during one-legged hopping, *J. Exp. Biol.* **208**, 4715–4725 (2005).
23. P. G. Weyand, M. W. Bundle, C. P. McGowan, A. Grabowski, M. B. Brown, R. Kram and H. Herr, The fastest runner on artificial legs: different limbs, similar function?, *J. Appl. Physiol.* **107**, 903–911 (2009).
24. W. H. Montgomery, M. Pink and J. Perry, Electromyographic analysis of hip and knee musculature during running, *Am. J. Sports Med.* **22**, 272–278 (1994).
25. G. Cappellini, Y. P. Ivanenko, R. E. Poppele and F. Lacquaniti, Motor patterns in human walking and running, *J. Neurophysiol.* **95**, 3426–3437 (2006).
26. S. C. Swanson and G. E. Caldwell, An integrated biomechanical analysis of high speed incline and level treadmill running, *Med. Sci. Sports Exercise* **32**, 1146–1155 (2000).
27. R. M. Alexander and A. S. Jayes, A dynamic similarity hypothesis for the gaits of quadrupedal mammals, *J. Zool.* **201**, 135–152 (1983).

## About the Authors



**Ryuma Niiyama** received his BA in Engineering from the University of Tokyo, Japan, in 2005, and his PhD in Interdisciplinary Information Studies from the University of Tokyo, in 2010. After graduation, he joined the Department of Mechano-Informatics at the University of Tokyo as a Postdoctoral Associate. He is currently a Postdoctoral Research Fellow at the Robot Locomotion Group, MIT CSAIL (Computer Science and Artificial Intelligence Laboratory). His current research interests are the design and control of bio-inspired machines.



**Satoshi Nishikawa** received his BA in Engineering from the University of Tokyo, Japan, in 2010. He is currently a Master's student at the Intelligent Systems and Informatics Laboratory in Interdisciplinary Information Studies, University of Tokyo, Japan. His current research interests are the dynamic motions of bio-inspired machines. He is a Student Member of the Robotics Society of Japan.



**Yasuo Kuniyoshi** is a Professor at the Department of Mechano-Informatics, School of Information Science and Technology, University of Tokyo, Japan. He received his PhD from the same University, in 1991, joined ETL, AIST, MITI, Japan, and moved to the current university, in 2001. His research interests include emergence and development of embodied cognition, humanoid robot intelligence, and machine understanding of human actions and intentions. He has published over 500 technical papers, and received the IJCAI 93 Outstanding Paper Award, Okawa Publications Prize, Gold Medal 'Tokyo Techno-Forum21' Award and other awards. He is a Member of the IEEE, SCJ, JSAI, IPSJ and JSBS.